Geoderma 401 (2021) 115163

Contents lists available at ScienceDirect

Geoderma

journal homepage: www.elsevier.com/locate/geoderma

Vis-NIR spectroscopy predicts threshold velocity of wind erosion in calcareous soils

Monireh Mina [a], Mahrooz Rezaei [a,b,*], Abdolmajid Sameni [a], Ali Akbar Moosavi [a], Coen Ritsema [c]

[a] Department of Soil Science, School of Agriculture, Shiraz University, Shiraz, Iran
[b] Meteorology and Air Quality Group, Wageningen University & Research, P.O. Box 47, 6700 AA Wageningen, the Netherlands
[c] Soil Physics and Land Management Group, Wageningen University & Research, P.O. Box 47, 6700 AA Wageningen, the Netherlands

ARTICLE INFO

Handling Editor: Cristine Morgan

Keywords:
Dust
Soil erosion
Spectral reflectance
Support vector machine
Wind tunnel

ABSTRACT

Wind erosion potential can be assessed using the Threshold Friction Velocity (TFV) of the soil, which is not always easy to measure, especially on regional and global scales. To overcome this difficulty, the spectroscopy technique can provide a useful approach in estimating the TFV as an alternative for time-consuming wind tunnel studies in the field. In this study, we evaluated the potential of Vis-NIR spectroscopy in predicting the TFV and some TFV-related soil properties using Partial Least Square Regression (PLSR) and the Support Vector Regression (SVR). We also developed a Point Spectrotransfer Function (PSTF) using Multiple Linear Regression (MLR) to predict the TFV based on diagnostic wavelengths and compared it to the derived Pedotransfer Function (PTF). For this purpose, 300 *in-situ* wind tunnel tests were performed in the Fars Province, Iran and the spectral reflectance of soil samples were analysed using a spectrophotometer apparatus. The 10 best key wavelengths resulting from the correlation analysis between the TFV and the spectral reflectance were 750, 1342, 1446, 1578, 1746, 1939, 2072, 2162, 2217, and 2338 nm which were mostly located in the short-wavelength infrared (SWIR) area. The derived PSTF performed better than the PTF for the TFV estimation ($R^2 = 0.94$, RMSE = 0.71). Results of the predictive models revealed that machine learning using the SVR had a significantly ($P < 0.01$) higher prediction accuracy for the TFV estimation ($R^2 = 0.85$, RMSE = 0.45, RPD = 2.50, and RPIQ = 4.06) than the PLSR ($R^2 = 0.68$, RMSE = 1.01, RPD = 1.72, and RPIQ = 2.64). The same results were obtained for the soil moisture, clay and $CaCO_3$ content. This study proved that reflectance spectroscopy coupled with the machine learning algorithm is a promising technique for large-scale assessment of wind erosion.

1. Introduction

Wind erosion is one of the main factors contributing to land degradation in arid and semi-arid regions (Pierre et al., 2014; Chappell et al., 2018) and it is a serious problem worldwide (Pásztor et al., 2016). Wind erosion occurs when both strong winds and soil erodible surfaces exist simultaneously (Chappell et al., 2018). Wind velocity must be large enough to carry soil particles; this is called the threshold friction velocity (TFV). TFV is considered to be a key parameter in specifying soil susceptibility in many wind erosion studies (de Oro and Buschiazzo, 2009; Li et al., 2015; Kouchami-Sardoo et al., 2019). Soil properties can influence TFV (Morshedi Nodej and Rezazadeh, 2018) and the severity of the wind erosion (Visser et al., 2004). The distribution of primary (textural) (Pásztor et al., 2016; Van Pelt et al., 2017; Kheirabadi et al., 2018) and secondary (aggregate) particles (Zamani and Mahmoodabadi, 2013), surface roughness (Yan et al., 2015), calcium carbonate content (Zobeck and Van Pelt, 2014, Kheirabadi et al., 2018, Kouchami-Sardoo et al., 2020), gypsum content (Tatarko, 2001, Ekhtesasi et al., 2003), and soil moisture (Zobeck and Fryrear, 1986; Ravi et al., 2006; Sirjani et al., 2019) are among the most important soil erodibility factors.

A fundamental challenge in controlling wind erosion is to accurately measure or predict TFV in arid and semi-arid areas (Okin, 2005). Over the last several decades, portable wind tunnels have been used to measure wind erosion in natural conditions for various purposes (Zobeck and Van Pelt, 2014). However, due to the time-consuming and difficulty of measuring TFV in the field, it would be advantageous if it could be estimated indirectly. This is especially important when dealing with large areas of wind erosion and aeolian sediment transport. Moreover, the spatial heterogeneity of TFV is difficult to estimate using a wind tunnel (Li et al., 2015). This is because a large number of wind

* Corresponding author at: Meteorology and Air Quality Group, Wageningen University & Research, P.O. Box 47, 6700 AA Wageningen, the Netherlands.
E-mail address: mahrooz.rezaei@wur.nl (M. Rezaei).

https://doi.org/10.1016/j.geoderma.2021.115163
Received 16 June 2020; Received in revised form 1 April 2021; Accepted 13 April 2021
Available online 27 April 2021

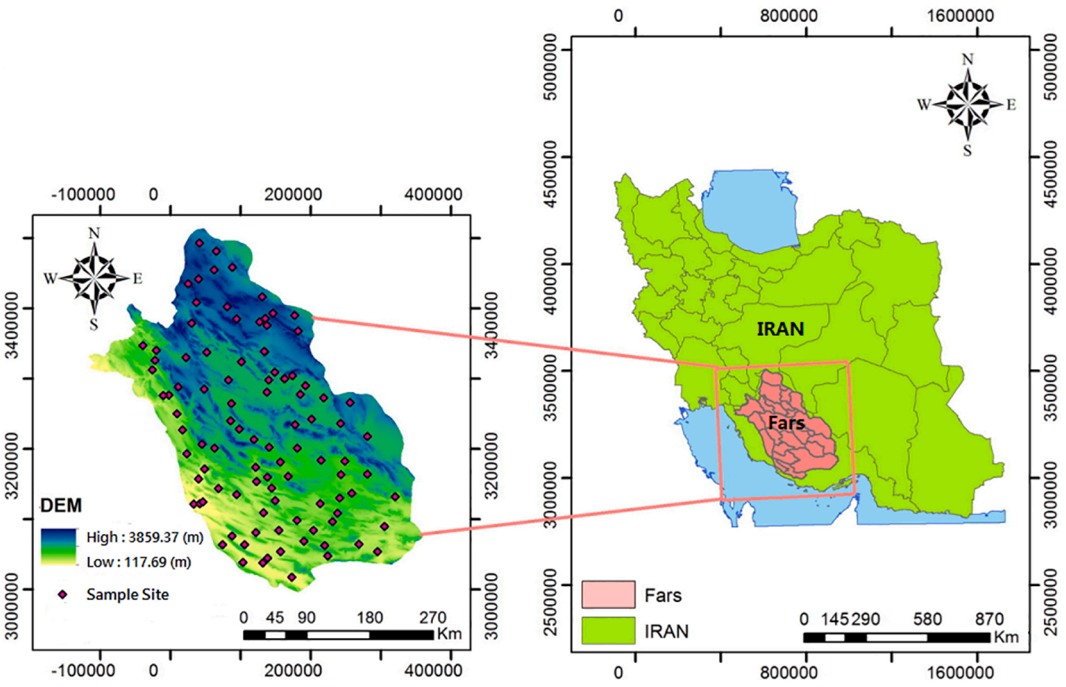

Fig. 1. Map of the Fars province in Iran with the geographical locations of the sampling sites (UTM, zone 39). DEM: Digital elevation model.

tunnel experiments are needed to cover the existing variability in soil surface conditions within an area of interest especially on large scale. Besides, the working section of the wind tunnel is not big enough to cover all these heterogeneities.

Visible-near infrared spectroscopy (Vis-NIR) is one of the most promising alternative techniques for routine soil analysis for total or partial replacement of traditional methods (Janik et al., 2009; de Santana et al., 2018). With the help of this technology, it is possible to estimate multiple soil properties simultaneously with a single measurement in the field or in the laboratory (Kim et al., 2014). In this regard, selection of the calibration method and its performance in modelling reflectance spectra is one of the main factors for calibration success (Mouazen et al., 2010). In most studies, linear multivariate calibration is used based on partial least square regression (PLSR). Using this method, we can determine the significant wavelengths associated with the desired variables from the measured wavelengths of each spectral curve. However, due to the complexity of the relationship between the spectra and wind erosion-related soil properties, PLSR may be insufficient thus other chemometric approaches mainly based on non-linear procedures should be considered. Machine learning algorithms are powerful methodologies for data modelling especially for complex non-linear systems (Nawar et al., 2016; de Santana et al., 2018). Once the diagnostic spectral bands are extracted, they can be used to estimate soil properties and then new functions, namely point spectrotransfer functions (PSTF), can be developed.

There has been only one study, conducted by Li et al. in 2015, that investigated the relationship between the TFV and the near and infrared spectral reflectance (350–2500 nm). They employed the PLSR method for TFV estimation due to the small number of samples (31 samples) (R^2 = 0.76, RMSE = 0.12). Their results identified the visible area (400–700 nm) and near infrared range (1100–2500 nm) as diagnostic wavelengths for estimating TFV. Ostovari et al. (2018) showed a good prediction (R^2 = 0.56) for estimating soil erodibility (K) in water erosion using the PLSR method in 40 samples. Apart from the direct relationship between soil erosion and soil spectra, there are some studies that have employed soil reflectance spectra to predict soil erosion-related properties. Wang et al. (2016) determined the factors governing soil erodibility using hyperspectral visible and near-infrared reflectance spectroscopy. These factors included water-stable aggregates (WSA), soil organic matter, and geometric mean diameter. They proved that a spectral analytical approach can be applied to complex datasets and provide new insights into emerging dynamic variations with erodibility estimations. Soil aggregate stability and aggregate size distribution were used as indicators of soil resistance to external erosive forces and were predicted using the Vis-NIR spectroscopic method (Shi et al., 2020). Soil organic matter (SOM) content was also used as a key indicator for determining water-induced soil erosion zones in Italy (Conforti et al., 2013) and in the Czech Republic (Žížala et al., 2017). Researchers employed the PLSR method as their calibration model and combined geostatistical approaches to map spatial patterns of the SOM. In another study, the shortwave infrared proximal sensing approach was used to quantify soil structure and aggregate stability as factors of soil resistance to water erosion (Gholoubi et al. 2018). Researchers found a strong correlation (r = 0.90) between the SWIR-derived reflectance index and the stability ratio of the soil. Schmid et al., (2012) used spectral characterization of land surface to determine soil erosion in Spain. In fact, they identified soil eroded areas based on a spectral characterization of morphological, physical and chemical features as a result of soil loss. In addition, spectral reflectance analysis was used in many studies to determine routine soil properties including the clay content (Peng et al., 2014), calcium carbonate equivalent (Bilgili et al., 2010; Summers et al., 2011; Khayamim et al., 2015a), organic carbon (Nawar et al., 2016; Sharififar et al., 2019), and cation exchange capacity (de Santana et al., 2018; Ng et al., 2019).

To the best of our knowledge, there has been no study on the application of Vis-NIR spectroscopy coupled with a machine learning algorithm to predict wind erosion. Such studies are needed for wind erosion controls and soil conservation efforts in large areas prone to wind erosion and dust emission like Iran. The results from this study can enhance the use of remote sensing in wind erosion studies on local and global scales. Therefore, the purpose of this study was 1) to evaluate the potential of the reflectance spectroscopy technique in estimating TFV, 2) to develop a point spectrotransfer function (PSTF) for TFV prediction, and 3) to compare PLSR and Support Vector Regression (SVR) models for optimal estimation of TFV using spectral reflectance.

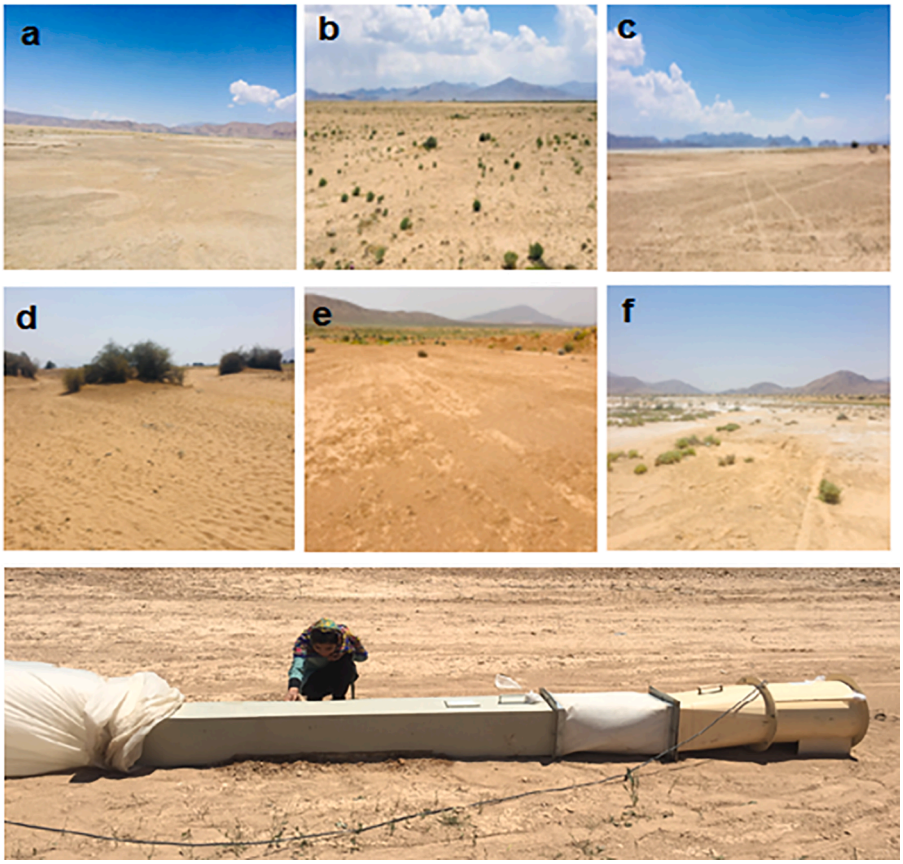

Fig. 2. General views of some study areas with the view of the wind tunnel set up in the field. a) 29° 47′ N and 53° 30′ E, b) 30° 30′ N and 53° 07′ E, c) 28° 13′ N and 53° 25′ E, d) 28° 11′ N and 52° 23′ E, e) 31° 01′ N and 52° 11′ E, and f) 28° 35′ N and 52° 23′ E.

2. Material and methods

2.1. Study area

The study area was Fars province which is located in the south central region of Iran (27°2′ to 31°42′ N and 50°42′ to 55°36′ E, covering an area of 133,299 km^2). Based on the De Marten aridity index, all parts of Fars province are classified as arid and semi- arid (Nafarzadegan et al., 2012). Due to the climate conditions of Fars province, wind erosion occurs in most areas. There are several critical wind erosion regions in this province (Rezaei, et al., 2016) and the three main dust-generating centres of the province are located in Abadeh (31° 11′ N and 52° 40′ E), Eghlid (30° 54′ N and 52° 38′ E), and Shiraz (29° 32′ N and 52° 36′ E). In this study, 100 sites in different geographical locations of Fars province were selected, providing a variety of soils with different physiochemical properties and thus different potential for wind erosion. Fig. 1 shows the geographical map of the sampling sites.

The maximum wind speeds vary between 7 and 30 m s^{-1} (at 10 m height) at Abadeh and Shiraz stations and between 7 and 45 m s^{-1} at Eghlid station. These high wind speeds are associated with west to southwest directions at Shiraz, southwest but also west and north directions at Abadeh, and southwest directions at Eghlid (Sirjani et al., 2019). A severe dust storm occurred in the province on May 13, 2018 (Aerosol optical depth value of 1.6). There were also several other events, for example on 17 July 1998, 13 August 2001, 24 April 2008, 28 February 2009, and 28 August 2013 with recorded wind speeds (at 10 m height) between 16 m s^{-1} and 20 m s^{-1} (Mazidi et al., 2015). The average annual rainfall in this province varies between 100 mm in the south and about 400 mm in the north.

The study area included seasonal and abandoned agricultural lands, rangelands, plains, and dried riverbeds and lakes. The slope of all the study areas was <1% and there was poor vegetation cover in all regions. General views of some of the study areas along with the view of the wind tunnel set up in the field are presented in Fig. 2.

2.2. Soil sampling and soil analysis

Soil samples were collected from the first 3 cm of topsoil at 100 study sites in the summer of 2019. Random soil samples were taken in triplicate from the places nearest to each of the wind tunnel runs. The collected samples were transferred to the laboratory and air-dried. In addition, one soil sample was weighed at each site using a scale and the sample was used for the initial soil moisture content. Soil texture was measured using the hydrometer method (Page et al., 1992). Soil chemical properties including $CaCO_3$ and $CaSO_4$ were measured using the back-titration and the acetone methods, respectively (Nelson, 1982).

2.3. Wind tunnel experiments

Information obtained from wind tunnel experiments forms a major part of wind erosion research (Shao, 2008). A detailed description of the wind tunnel used in this study can be found in Rezaei et al. (2019). Extensive *in-situ* wind tunnel experiments were performed at 100 selected study sites. Three distinctive places were identified for wind tunnel experiments at each study site. In total, 300 wind tunnel experiments were carried out for this study. All three replications (mean STD = 0.26) were done on the same surface type as close to each other as possible, but not overlapped with footprints of previous wind tunnel tests, as the wind tunnel test would cause disturbance to the soil surface. At each site, wind tunnel experiments were carried out on flat areas of

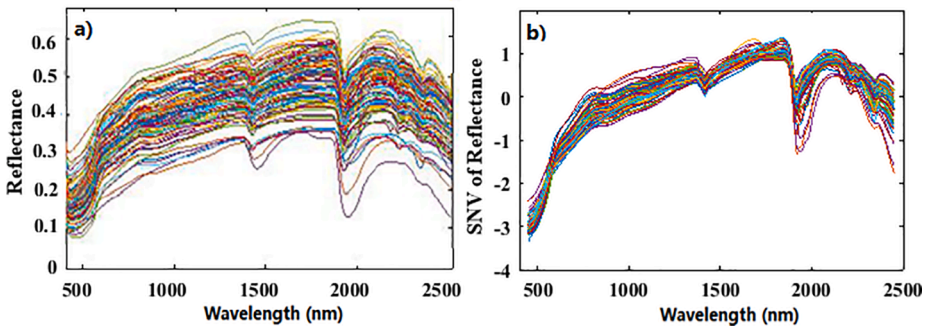

Fig. 3. The a) raw and b) pre-processed spectral reflectance data of the soils (n = 100) in the study area.

land with little to no vegetation, rocks or rubble and without any surface disturbance. After determining the appropriate test points, the wind tunnel was positioned on intact soil in the direction of the prevailing wind. Threshold wind erosion velocity was measured using the observational method by gradually increasing the velocity of wind in the wind tunnel until the forward movement of the soil particles was observed (Belnap et al., 2007; Rezaei at al., 2019). It might be worth to mention that each wind tunnel experiment took at least 90 min including the replicates at each study site. The whole field work of the study was carried out in 25 days.

2.4. Spectral reflectance measurement

The spectral reflectance of the soil samples was collected using a spectrophotometer apparatus (Metrohm, NIRS XDS, RapidContent Analyzer) in Vis-NIR range (400–2500 nm) with 0.5 nm data point interval (4200 wavelengths), <0.05 nm wavelength accuracy and 8.75 nm bandpass. The spectrophotometer measures the reflectance using two detectors (Si detector and PbS detector) which caused a splice in the wavelengths of 1099–1100 nm. Therefore, a splice correction was employed on the spectral reflectance. Soil samples were air-dried and sieved through a ≤2 mm sieve. Soil material (~25 g) was then placed in a container and thoroughly mixed before analysis. Twenty scans were considered for each soil sample in order to get an average reflectance spectrum. The spectral regions of 400–449 nm and 2451–2500 nm were removed in order to eliminate the influence of noise. In other words, the reflectance spectra after noise reduction were in the range of 450–2450 nm. In order to eliminate turbulence and to increase the quality of the spectral data, pre-processing methods were performed. Kuśnierek (2011) reported a 30% increase in accuracy by using different pre-processing methods compared to non-pre-processing conditions. Therefore, the Savitzky-Golay filter (SG) (Savitzky and Golay, 1964) was used on all spectral data with a zero-order filter, polynomial of 2nd order and 15 smoothing points. Then, the standard normal variate (SNV) method for each parameter was carried out as a spectral pre-processing algorithm. The Unscrambler X v. 10.4 software (Camo Software AS, Oslo, Norway) was used for spectral data processing. Fig. 3 provides the raw (a) and pre-processed (b) spectral reflectance of the 100 soil samples.

2.5. Development of pedotransfer function (PTF) and point spectrotransfer function (PSTF) to predict TFV

PTF and PSTF were developed by considering the correlation between the soil properties or initial spectral wavelengths and TFV. The multiple linear regression (MLR) analysis was used for PTF and PSTF development. MLR is a regression method in which two or more independent variables are used to analyse a dependent variable. In this research, clay, sand, silt, Gravimetric Soil Moisture (GSM), $CaSO_4$, and $CaCO_3$ were included in the regression model. Given that the most important principle in modelling is to provide a simple model with a low number of input variables and high efficiency, stepwise regression was used to select the best combination of independent variables as model inputs. Moreover, high levels of multicollinearity between variables could lead to over-fitting of the model. Therefore, the Variance Inflation Factor (VIF) was used and variables with a VIF value >5 were removed from the model (Ostovari et al., 2019). The F test was used to test the significance of the regression model at the probability level of 5%. If the regression model was significant, its coefficients were analysed using the *t*-test.

Likewise, the effective spectra for the development of PSTF were selected and the stepwise multiple linear regression (MLR) was employed to derive PSTF and predict TFV.

For MLR, the samples were randomly divided into calibration and validation datasets. The calibration dataset (70%) was used for model development and the validation dataset (30%) was used for evaluating the developed function. Statistical analyses were run by SPSS 16 software. Performance of PTF and PSTF were analysed based on the coefficient of determination (R^2), the root mean squared error (RMSE), and standard deviation (STD) of the measured data. Any RMSE values less than half the standard deviation of the actual data were considered good (Singh et al., 2005; Moriasi et al., 2007).

2.6. Statistical analysis and predictive models

One of the problems in processing spectral data is due to the collision effect of different factors in each wavelength and repeated information in adjacent wavelengths. When predictive variables are greater than the measured samples (i.e., 400–2500 spectral wavelengths versus 100 soil samples in the present study), the degree of overlapping will increase and it will cause overfitting. For such data, a multivariate analysis should be conducted to determine the most important variables (Abbasi et al., 2011; Hong et al., 2018). To predict TFV based on the spectra, a multivariate regression and a machine learning algorithm were implemented, including partial least squares regression (PLSR) (Haaland and Thomas, 1988) and support vector regression (SVR) (Vapnik, 1995). PLSR is based on linear least squares regression that performs with new components instead of the original input data. The predictors are reduced to principal components, as are the dependents (Abbasi et al., 2009). In PLSR, the compression and regression steps are integrated and the new latent variables (LV) by reducing dimensional space and noise of spectral variables are determined (Wan et al., 2019). LVs (range 1–15) which were used to optimize the covariance between soil properties and spectra in PLSR, were determined after the minimum RMSE was obtained using holdout cross-validation. Then the extracted LVs were used as the linear combination of the predictor variables.

SVR, on the other hand, has special features for dealing with complex multidimensional data. SVR forms a supervised learning model with machine learning algorithms that analyses the data used for regression analysis. In this study, the kernel and type of SVR were set as linear function and epsilon-SVR, respectively. The penalty parameter (C) (range $1e^{-3}$-$1e^{3}$) that controls the distance from epsilon was acquired

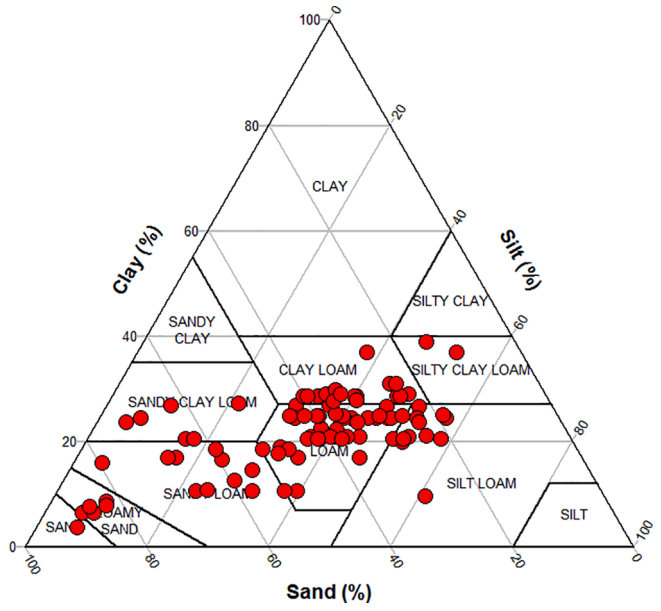

Fig. 4. The USDA textural distribution of the soils at the study sites.

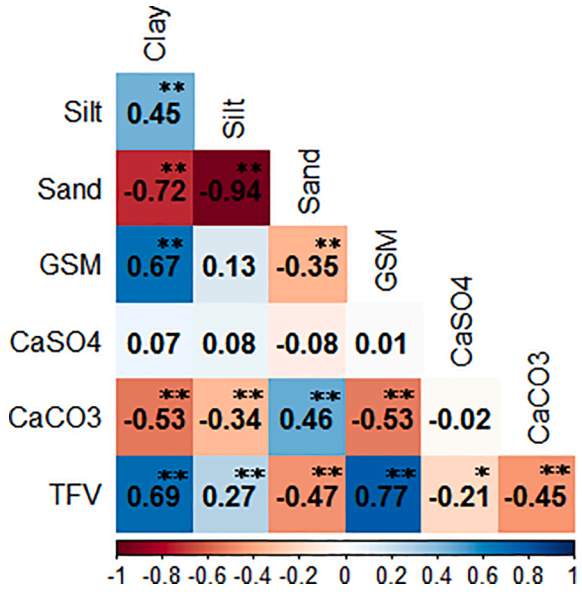

Fig. 5. Pearson correlogram of soil physiochemical properties and TFV. GSM – Gravimetric Soil Moisture, TFV – Threshold Friction Velocity. Superscripts * and ** represent $p < 0.05$ and $p < 0.01$, respectively.

using a systematic grid search technique, and the optimal parameters were determined after the minimum RMSE was obtained using holdout cross-validation.

PLSR and SVR models were performed to establish the relationship between soil parameters and spectral data matrix using the PLS Toolbox version 8.02 (Eigenvector Research, Inc., Wenatchee, WA, USA) and LIBSVM (Chang and Lin, 2011), in MATLAB2019b programming environment.

2.7. Model evaluation and comparison

Calibration models were developed based on the spectral range 450–2450 nm using PLSR and SVR regression. In this study, 100 samples were randomly divided into calibration (70%) and validation datasets (30%). The Student's *t*-test was used to examine the mean difference between calibration and validation datasets for spectral analysis. The efficiencies of the predictive models were then evaluated using the coefficient of determination (R^2), root mean squared error (RMSE), the ratio of predicted deviation (RPD), and ratio of performance to the interquartile range (RPIQ).

The estimations were classified as: very poor with RPD < 1, weak with RPD = 1–1.4, moderate with RPD = 1.4–1.8, good with RPD = 1.8–2, very good with RPD = 2–2.5, and excellent with RPD > 2.5 (Lacerda et al., 2016). The same classification was applied for the RPIQ analysis.

In order to compare the model performances statistically, we used the randomization *t*-test (van der Voet, 1994) for RMSE values resulting from 100 model simulations. These simulations were run (with different random calibration and validation datasets) for each of the parameters and each of the two predictive models separately and were used for the significance tests. The hypotheses evaluated were:

H0) Null hypothesis: $RMSE_A = RMSE_B$ (the predictive accuracy of model A and model B are equal); H1) Alternative hypothesis: $RMSE_A \neq RMSE_B$ (the predictive accuracy of model A and model B are not equal).

Statistical analysis and modelling were performed using the Machine Learning Toolbox in MATLAB 2019b.

3. Results and discussion

3.1. Soil properties

Soil textural distributions of all the study areas are presented in Fig. 4. With eight different soil texture classes, we studied a large panel of different soil types that can be found in southern Iran, confirming a variety of soils with different potential for wind erosion. The statistical summary for some important soil properties and TFV is shown in Table 1. The clay, silt, and sand contents varied with a coefficient of variation very close to each other (30%, 39%, and 43%, respectively). Furthermore, gravimetric soil moisture contents were low with an average of 1.11%. This soil moisture was below the highest soil moisture allowed to guarantee wind erosion (Nourzadeh et al., 2013, Bento et al., 2017). The $CaCO_3$ content showed the lowest coefficient of variations (15%) among all soil properties, indicating a low variation (0–15% according to Wilding, 1985) in the study area which is related to the calcareous parent materials in Iran. Moreover, the variation of gypsum

Table 1
Statistical analysis of the soil properties and TFV.

Soil property	Min.	Q1	Median	Mean	Q3	Max.	STD	CV (%)
Clay (%)	3.72	12.60	23.7	22.1	26.6	38.9	6.74	30
Silt (%)	4.64	31.10	37.5	35.8	45.8	60.7	13.89	39
Sand (%)	10.6	28.72	37.1	41.9	50.7	89.5	17.95	43
GSM (%)	0.00	0.75	1.07	1.11	1.37	2.48	0.65	58
$CaSO_4$ (%)	0	0.67	0.71	0.92	0.82	3.98	0.69	75
$CaCO_3$ (%)	35.9	47.77	52.2	57.7	61.3	83.5	9.02	15
TFV (m s^{-1})	1.50	6.00	7.50	7.21	8.00	12.5	1.98	28

GSM – Gravimetric Soil Moisture, TFV – Threshold Friction Velocity, Q1 – First quartile, Q3 – Third quartile, STD – Standard Deviation, CV – Coefficient of Variation, where < 15% = low variability, 15–35% = moderate variability, >35% = high variability (Wilding, 1985).

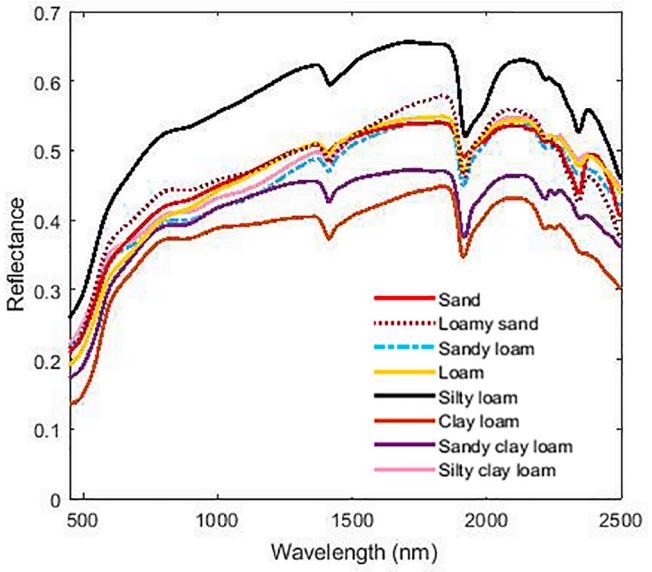

Fig. 6. Changes in spectral reflectance for soil textural classes.

content was very large with the highest CV of 75%. Average TFV ranged from 1.50 to 12.5 m s^{-1}, showing a very different potential for wind erosion across the study area.

The Pearson's correlation coefficient ($P < 0.05$) between the measured soil physiochemical properties and the TFV is shown in Fig. 5. The TFV had the highest correlation ($r = 0.77$) with soil moisture. TFV is very sensitive to soil moisture (Shao and Lu, 2000) as soil moisture strengthens the adhesion forces between the soil particles and increases the resistance of soil particles to wind erosion (Wiggs et al., 2004). In fact, the capillary force between the particles is the main factor for increasing the TFV with increasing moisture (Berg et al., 2007).

Among soil texture components, the percentage of clay had the highest correlation ($r = 0.69$) with TFV. According to Bonilla and Johnson (2012), clay components are less susceptible to erosion and more resistant to deterioration by the eroding agent due to their small size as well as the adhesion force between particles. Thus, an increase in the clay content of the soil can increase soil resistance against erosive forces (Carrick et al., 2010).

Moreover, TFV showed a relatively high negative correlation with $CaCO_3$. Chepil (1954) also showed that an increase in calcium carbonate caused a substantial disintegration of soil cloddiness and a decrease in the stability of clods in soils of arid areas other than sands and loamy sands. Considering that the study area is located in a dry region with a high amount of lime, the negative correlation between $CaCO_3$ and TFV is described.

3.2. Characteristics of spectra

Representative soil spectra showed three specific absorption bands at 1414, 1915, and 2212 nm (Fig. 6). These absorption characteristics also demonstrate free and hygroscopic water at 1414 nm, hydroxyl groups at 1915 nm, clay mineral networks, the bonding of hydroxides with iron, magnesium and aluminium metals at 2212 nm (Clark et al., 1990). The absorption peaks around 2341 nm are related to CO_3 groups in carbonate minerals (Gomez et al., 2008, Lagacherie et al., 2008). In addition, spectral curves have a peak at wavelengths of 500 to 700 nm which can be attributed to goethite and hematite in the soil (de Santana et al., 2018).

Fig. 6 shows the variation in the spectral reflection value in the presence of eight different soil texture classes including sand, loamy sand, sandy loam, loam, silty loam, clay loam, sandy clay loam, and silty clay loam. Clay loam and sandy clay loam classes have the least

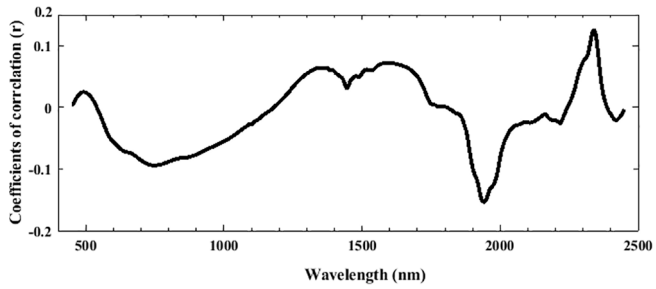

Fig. 7. Pearson's correlation coefficient (r) between spectral reflectance values across the Vis-NIR range and threshold friction velocities (TFVs).

reflectance. In fact, as the clay content increases, the spectral reflectance decreases (Wang et al., 2017). This reduction in the reflectance is due to the presence of clay and phyllosilicates. The smaller the size of the soil particles, the higher the surface and the presence of clay minerals and iron, manganese, and aluminium oxides (Yan et al., 2016). On the other hand, silt loam class shows the highest reflection due to the presence of bright minerals such as calcites and carbonates. Iron oxides affect the reflection in the visible region, whereas organic carbon and clay affect the amount of reflection in the infrared region (Babaeian et al., 2015). Regarding the effect of soil texture on spectral reflectance, it can be stated that sandy soils have higher light scattering than clayey soils and thus they have higher reflection compared to fine-textured soils (Stevens et al., 2013).

3.3. Correlation analysis between TFV and spectral reflectance

The Pearson correlation coefficient between the spectral reflectance and TFV in the range of 400–2500 nm is illustrated in Fig. 7. It can be used to identify the most important bands and, later, to develop PSTF for predicting TFV. As can be seen in Fig. 7, there is a relatively high correlation between the measured values of TFV and the soil spectral reflectance. In general, the relationship between spectra and TFV appeared in diagnostic bands of around 1400, 1900, and 2200 nm. These results are consistent with experimental studies that show the relationship between TFV and soil properties (Kouchami-Sardoo et al., 2019).

The TFV showed the highest significant correlation ($P < 0.05$) with spectral bands at 750, 1342, 1446, 1578, 1746, 1939, 2072, 2162, 2217 and 2338 nm. Li et al. (2015) reported a significant correlation ($P < 0.05$) for wavelengths of 517–543, 1347–1354, 1898–1911, 1936–1943, 1969–2092, 2273–2293 with TFV which were proportional to the fine soil content and consistent with our results. It can be concluded that the SWIR area has a promising role in wind erosion studies.

Considering the high correlation between soil moisture content and TFV ($r = 77\%$, see Fig. 5), the significant correlation between TFV and bands of 1342, 1446, 1939, and 2217 nm can be described accordingly. There are three spectrally active forms of water in the soil; free water, adsorbed water, and hydration water (Ben-Dor, 2002). Diagnostic water adsorption features are centred around 1440, 1930, and 2200 nm (Knadel et al., 2014). These wavelenghts are associated with free water OH features at 1400 and 1900 nm and clay lattice OH features at 1400 and 2200 nm (Vicente and de Souza Filho, 2011). Adsorbed water (a thin layer on the surfaces of clay minerals) has an absorption band around 2200 nm. Hydration water is incorporated into the mineral lattice with two strong OH absorption features near 1440 and 1930 nm (Knadel et al., 2014). The wavelengths of 1360 and 1940 nm were also used for the Normalized Soil Moisture Index (NSMI) as a proxy of soil moisture (Hong et al., 2018). It would be interesting to note that the correlation between TFV and spectral reflectance at wavelength of 1900 nm was negative, while such correlation was positive at around 1400 nm (see Fig. 7). These wavelengths are associated with both free and hydration water. As our soil samples were air-dried, the effect of free water can be neglected. Therefore, such correlation can be related to hydration

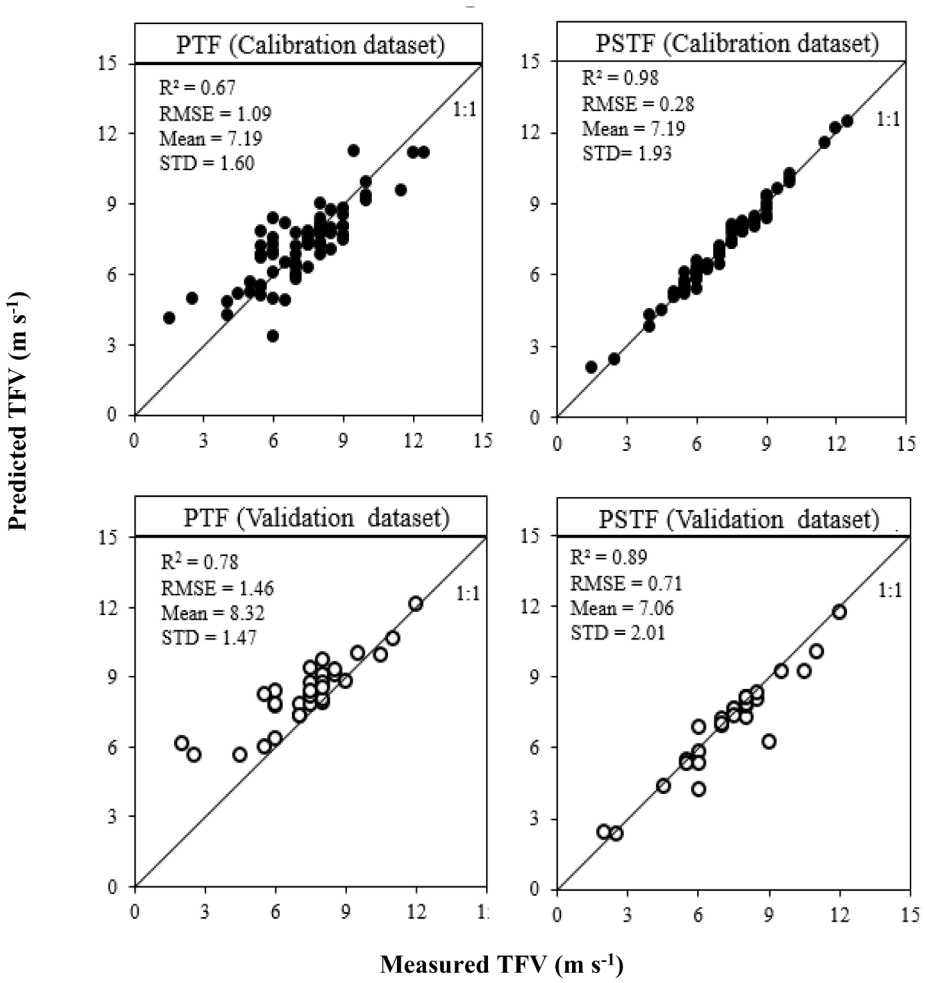

Fig. 8. Performances of pedotransfer function (PTF) and point spectrotransfer function (PSTF) for Threshold Friction Velocity (TFV) for the calibration dataset (top) and validation dataset (bottom).

water that is incorporated into mineral lattice and is related to the clay mineralogy of the soil samples. For instance, the 1900 nm is more pronounced in expandable clay minerals (Vicente and de Souza Filho, 2011).

Likewise, based on the correlation between clay and TFV (r = 69%, see Fig. 5), a high correlation was observed between TFV and bands of 1578, 2072, 2217, and 2338 nm. An increase in clay content results in a more pronounced adsorption feature at 2200 nm (Nawar et al., 2016). Babaiean et al. (2015) also introduced the wavelengths of 1827 and about 2300 nm in a model to estimate the clay content. Wavelengths around 2340 nm can also represent illite or mixtures of muscovite minerals (Post and Noble, 1993). Wavelengths of around 1600, 2000, and 2100 nm were also introduced for clay content estimation by Viscarra Rossel and McBratney (1998).

As is clearly shown in Fig. 7, maximum correlation between TFV and spectral reflectance is related to the wavelength of 2338 nm which can be described by the presence of calcium carbonate equivalent in the soil. The negative correlation between calcium carbonate equivalent and TFV (see Fig. 5) is indicative of this point. A wavelength at around 2340 nm was reported as a diagnostic absorption spectrum in many studies which is related to the vibration of the CO_3 group of soil (Rossel et al., 2006; Khayamim et al, 2015a; Kumar & Yarrakula, 2019). The correlation of TFV with the wavelength of 1578 nm can be attributed to the amount of gypsum (Khayamim et al., 2015b).

3.4. PTF and PSTF development for predicting TFV

The stepwise multiple regression analysis showed that soil moisture (P = 0.00, VIF = 1.86), clay content (P = 0.001, VIF = 1.86), and gypsum content (P = 0.00, VIF = 1.00) were strongly related to TFV values. The VIF for these parameters was lower than 5, indicating a discrepancy between the input variables. Although from the Pearson correlation we did not find a strong relationship between TFV and $CaSO_4$ (r = −0.21), $CaSO_4$ was significant in MLR analysis. This is statistically meaningful as a suppressive variable which increases the predictive validity of another variable by its inclusion in a regression equation. The underlying relationship between TFV and soil properties is as follows.

$$TFV = 4.04 + 1.47(GSM) - 0.74(CaSO_4) + 0.09(Clay) + 1.13 \quad (1)$$

where TFV is threshold friction velocity (m s^{-1}), GSM (%) is the

$$TFV = 5.74 + 19.51R_{750} - 112.35R_{1342} - 58.30R_{1446} + 227.61R_{1578} - 38.22R_{1746} - 32.77R_{1939} - 118.54R_{2072} + 89.38R_{2162} - 55.04R_{2217} + 86.45R_{2338} + 0.48 \quad (2)$$

Table 2
Prediction results for clay, Gravimetric Soil Moisture (GSM), carbonate content ($CaCO_3$), and Threshold Friction Velocity (TFV) using partial least squares regression (PLSR) and support vector machine (SVR) algorithms.

Model	Soil Properties	Calibration		Validation			
		R^2	RMSE	R^2	RMSE	RPD	RPIQ
PLSR	Clay (%)	0.68	0.11	0.54	0.21	1.46	1.84
	GSM (%)	0.81	0.37	0.64	0.32	1.61	2.46
	$CaCO_3$ (%)	0.84	4.58	0.72	5.32	1.86	2.96
	TFV (m s^{-1})	0.88	0.70	0.68	1.01	1.72	2.64
SVR	Clay (%)	0.82	0.07	0.74	0.04	1.75	2.35
	GSM (%)	0.92	0.10	0.78	0.14	2.10	3.04
	$CaCO_3$ (%)	0.97	1.84	0.82	2.09	2.13	3.37
	TFV (m s^{-1})	0.94	0.45	0.85	0.45	2.50	4.06

R^2 – Coefficient of determination, RMSE – Root Mean Squared Error, RPD – Ratio of Predicted Deviation, and RPIQ – Ratio of Performance to the Interquartile Range.

gravimetric soil moisture, $CaSO_4$ is gypsum content (%), and Clay shows clay content (%).

Likewise, we selected the effective spectra for the development of PSTF based on the correlation between wavelengths (400–2500 nm) and TFV using Fig. 7. The selected spectra were significant at the 5% level of confidence and had the highest correlation with TFV. Eq. (2) provides the created PSTF for estimating TFV based on spectral reflectance.

In this equation, R_x is the initial spectral reflectance at a specified wavelength (x). At these wavelengths, moisture, clay, and $CaCO_3$ diagnostic bands are detectable. Considering the positive and negative significant correlation between TFV and these soil properties, the employment of these spectra is reasonable. In other words, these spectral bands are consistent with those of the known variables that have a significant impact on TFV. Fig. 8 shows the values of measured versus predicted TFV using PTF (Eq. (1)) and PSTF (Eq. (2)) for the calibration and validation datasets. This figure indicates that the predicted and

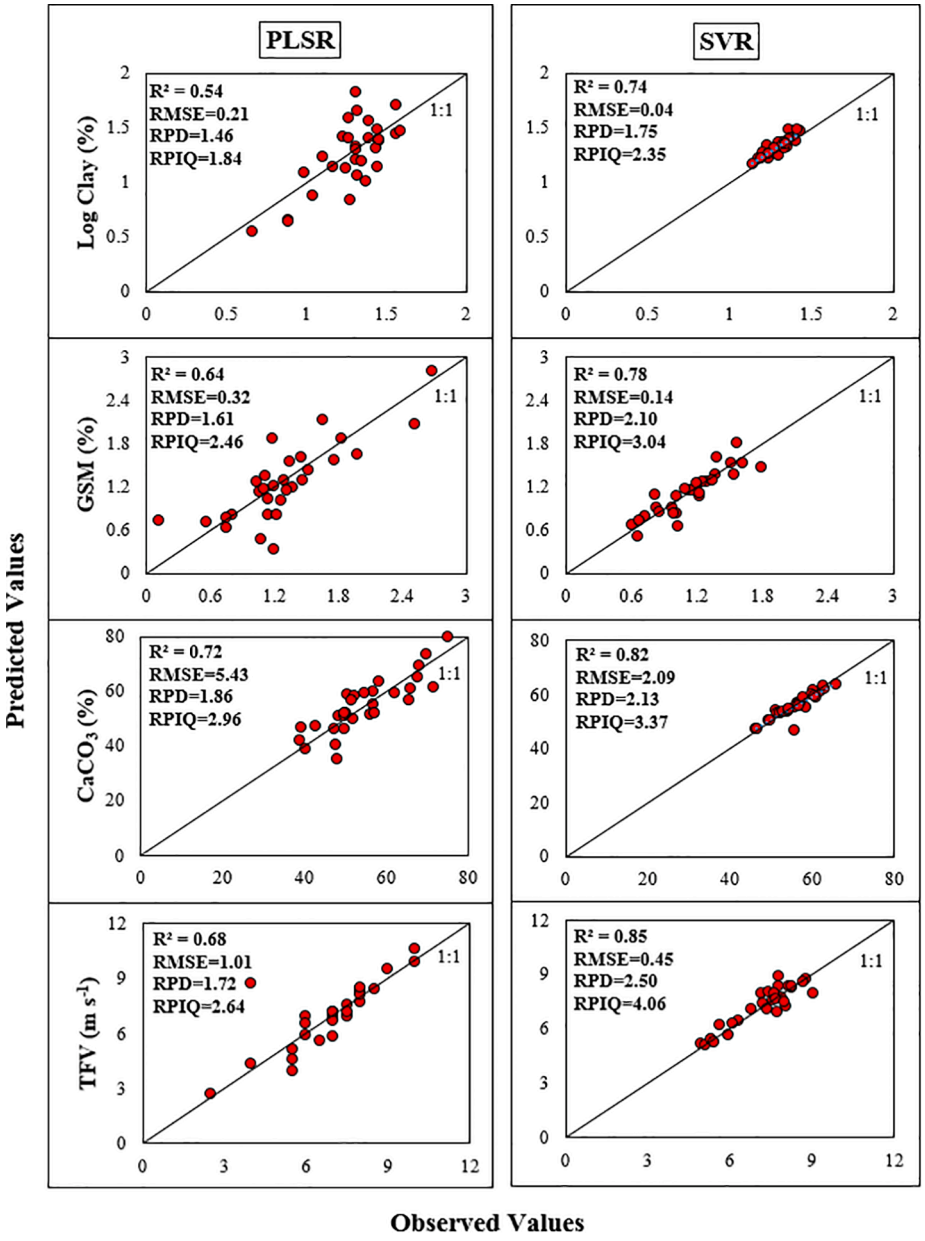

Fig. 9. Scatter plots of predicted versus measured log clay, gravimetric soil moisture (GSM), carbonate content ($CaCO_3$), and threshold friction velocity (TFV) by partial least squares regression (PLSR) and support vector machine (SVR) models.

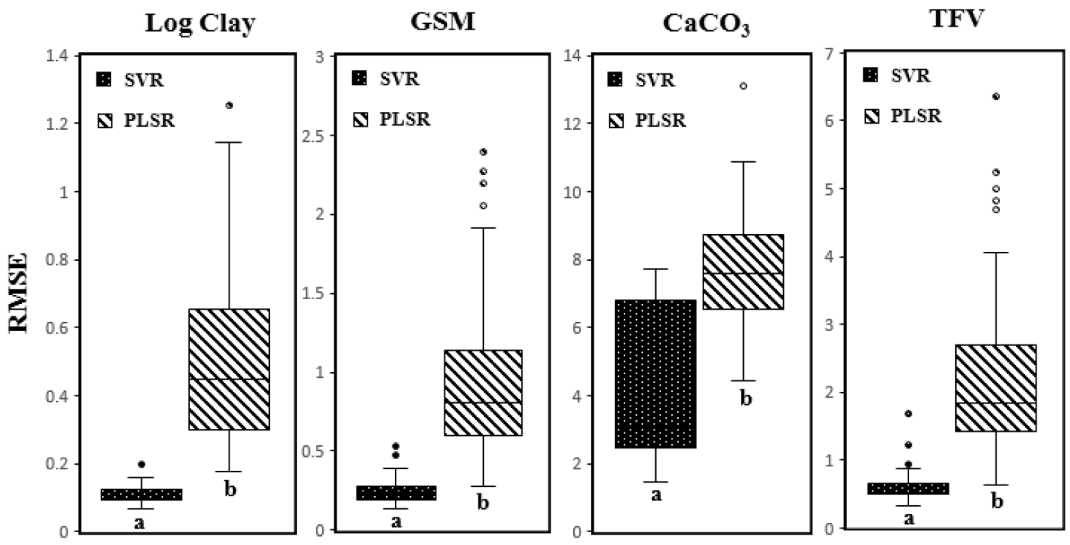

Fig. 10. Boxplots of RMSE resulting from 100 replicated simulations using partial least squares regression (PLSR) and support vector machine (SVR) models for each parameter together with their significance statistics ($P < 0.01$). Models followed by different letters are significantly different.

measured TFVs are largely consistent.

As is clearly shown in Fig. 8, in both calibration and validation data sets, PSTF ($R^2 = 0.98$, RMSE = 0.28 for calibration and $R^2 = 0.89$, RMSE = 0.71 for validation data sets) showed higher performance than PTF. The low values of RMSE obtained for the calibration (RMSE = 0.28) and validation (RMSE = 0.71) data for PSTF and comparing them with the standard deviation of the measured data (STD = 1.93 for calibration and STD = 2.01 for validation data) reveals the acceptability of these spectral functions for the prediction of TFV based on key wavelengths (Singh et al., 2005; Moriasi et al., 2007). Considering the cost and time involved in soil sampling and experimental measurements of soil properties such as gypsum content and the promising accuracy of the derived PSTF, the application of PSTF for wind erosion studies on the local as well as the global scale has been proved.

3.5. Prediction of clay, GSM, $CaCO_3$, and TFV

Results of all models for clay, GSM, $CaCO_3$, and TFV prediction using spectral reflectance are summarized in Table 2. Fig. 9 also presents the scatter plots illustrating predicted versus measured clay, GSM, $CaCO_3$, and TFV using PLSR and SVR approaches. The concentration of all parameters are distributed along the adjusted regression line in the validation group. The results indicate the acceptability of the estimate, since the predicted and measured values are largely consistent. Overestimated and underestimated predicted values with respect to RMSE and RPD were not seen to the extent that the regression model was invalidated.

Model performances were assessed using datasets that were not included in the calibration as the external validation set. Comparing the two models for TFV, the SVR model showed the largest R^2 (0.85) and the lowest RMSE (0.45), with RPD of 2.50 and RPIQ equal to 4.06 proving an excellent prediction compared to the PLSR model ($R^2 = 0.68$, RPD = 1.72). For clay, GSM, and $CaCO_3$, the same trend in the accuracy of models was observed with SVR being the most accurate model. It showed $R^2 = 0.74$ (RPD = 1.75), $R^2 = 0.78$ (RPD = 2.10), and $R^2 = 0.82$ (RPD = 2.13) for clay, GSM, and $CaCO_3$, respectively.

The performance of PLSR in the prediction of TFV was estimated ($R^2 = 0.76$, RMSE = 0.12) in a study by Li et al. (2015). The difference in the accuracy factors can be related to the lower number of samples (31) compared to ours (100 samples).

The results of our study for clay was consistent with previous studies showing the superior performance of the SVR model compared to PLSR (Kovačević et al., 2010; Rossel and Behrens, 2010, Terra et al., 2015; Dotto et al., 2017; Campbell et al., 2018; Raj et al., 2018). The results of our study indicate that the data mining techniques (SVR) outperform the PLSR method because of their ability to include nonlinear interactions and relationships as was reported in other studies (Brown et al., 2006; Mouazen et al., 2010; Rossel and Behrens, 2010; Vohland et al., 2011; Raj et al., 2018). The superior performance of the machine learning model compared to PLSR to quantify clay content was also reported by de Santana et al. (2018) who related this to the lower number of outliers excluded in calibration and validation sets as compared to PLSR. For $CaCO_3$, a similar R^2 (0.71) and RPD (1.6) were reported using PLSR by Ostovari et al. (2018).

Although the initial results showed that SVR is the best model for TFV prediction (Table 2), it is statistically important to test whether the difference between R^2 or RMSE values of the two models are significant. Thus, the p-values from randomization *t*-test of the two models were compared for TFV and related soil properties estimation. Fig. 10 presents the boxplots of RMSE values for the two models with 100 replicated simulations. The difference between the PLSR and the SVR models for prediction of TFV, GSM, and $CaCO_3$ were significant ($P < 0.01$). This proves that the SVR model has a higher predictive accuracy and is a superior model to quantify TFV. SVR has better performance in modelling and better establishment in nonlinear relationships between soil properties and reflectance spectra (Stenberg et al., 2010).

Thus, better performance of SVR compared to PLSR may be related to the soil complexity and nonlinear behaviour of the soil variables (Xu et al., 2018).

Generally, by increasing the numbers and the variability of samples, predictive capabilities of models tend to become more complex. Machine learning calibration models can increase the accuracy of prediction in such circumstances. In general, for a soil property like TFV that has no well-identified spectral feature, the machine learning algorithms can have better performance. It would be worth to mention that SVR has no inherent capacity to perform feature ranking and does not reveal functional relationships between the target and the predictor variables (Taghizadeh-Mehrjardi et al., 2016; Xu et al., 2018). These limitations in comprehension and interpretation are the reasons SVR is considered as the "black box" approach (Rossel and Behrens, 2010). Therefore, this uninterpretable characteristic should be taken into account when using machine learning algorithms.

The results of the predictive models confirm that the use of spectroscopy is very useful for estimating soil properties, especially soil erosion related parameters. More importantly, reflectance spectroscopy provides a quick, non-invasive and non-destructive method for collecting information about soil, a technique that can be a valuable tool for

estimating TFV. Fieldwork in vast areas with dry and hot conditions but also prone to wind erosion (like Fars province) is very costly and time-consuming which can limit the researches done in this field. It is noteworthy that due to the heterogeneity of the soil, more efforts are still needed to develop calibration models.

4. Conclusion

In this study, we explored the ability of reflection spectroscopy to estimate TFV in wind erosion studies. Generally, the results showed that there is a significant correlation between the TFV and soil spectral reflectance. Wavelengths of 1400, 1900, 2200, and 2338 nm were presented as the key spectral bands for TFV prediction. In addition, using MLR analysis, a new PSTF was proposed which showed a higher accuracy than the developed PTF. Among the two predictive models, the machine learning algorithm performed better compared to the common PLSR method. SVR was introduced as the best algorithm for TFV and three TFV-related properties (clay, $CaCO_3$, and soil moisture) estimations. Our results proved that spectral reflectance is a promising tool for efficiently assessing large areas prone to wind erosion and dust emission.

It should be noted that this study gives the first look at the role of spectroscopy coupled with a machine learning algorithm in wind erosion. These spectra can be recorded from other platforms such as remote sensing. Therefore, to get a better understanding of its application, a further study extending the developed PSTF using satellite imageries for spatial distribution of TFV is recommended. The encouraging point is that upcoming satellite hyperspectral imagers will provide high-resolution Vis-NIR spectral data across large spatiotemporal scales (Shi et al., 2020). In addition, we recommend using a portable spectrophotometer in the field for future studies in order to increase the accuracy of the spectral data obtained from intact soil.

Declaration of Competing Interest

The authors declare that they have no known competing financial interests or personal relationships that could have appeared to influence the work reported in this paper.

References

Abbasi, M., Darvishsefat, A.A., Schaepman, M.E., Mohdjer, M.R.M., Sobhany, H., 2009. Investigation on leaf spectral reflectance of most important species of Caspian forests using field Spectroradiometry. Iran. J. For. Poplar Res. 17 (4), 568–580.

Abbasi, Y., Ghanbarian-Alavijeh, B., Liaghat, A.M., Shorafa, M., 2011. Evaluation of pedotransfer functions for estimating soil water retention curve of saline and saline-alkali soils of Iran. Pedosphere 21 (2), 230–237.

Babaeian, E., Homaee, M., Montzka, C., Vereecken, H., Norouzi, A.A., 2015. Towards retrieving soil hydraulic properties by hyperspectral remote sensing. Vadose Zone J. 3–14.

Belnap, J., Phillips, S.L., Herrick, J.E., Johansen, J.R., 2007. Wind erodibility of soils at Fort Irwin, California (Mojave Desert), USA, before and after trampling disturbance: implications for land management. Earth Surf. Process. Landforms: J. Br. Geomorphol. Res. Group 32 (1), 75–84.

Ben-Dor, E., 2002. Quantitative remote sensing of soil properties. Adv. Agron. 75, 173–243.

Bento, C.P., Goossens, D., Rezaei, M., Riksen, M., Mol, H.G., Ritsema, C.J., Geissen, V., 2017. Glyphosate and AMPA distribution in wind-eroded sediment derived from loess soil. Environ. Pollut. 220, 1079–1089.

Berg, D.E., Zayas, J.R., Lobitz, D.W., van Dam, C.P., Chow, R., Baker, J.P., 2007. In: Active aerodynamic load control of wind turbine blades. American Society of Mechanical Engineers Digital Collection, pp. 1119–1127.

Bilgili, A.V., Van Es, H.M., Akbas, F., Durak, A., Hively, W.D., 2010. Visible-near infrared reflectance spectroscopy for assessment of soil properties in a semi-arid area of Turkey. J. Arid Environ. 74 (2), 229–238.

Bonilla, C.A., Johnson, O., 2012. Soil erodibility mapping and its correlation with soil properties in Central Chile. Geoderma 189–190, 116–123.

Brown, D.J., Shepherd, K.D., Walsh, M.G., Mays, M.D., Reinsch, T.G., 2006. Global soil characterization with VNIR diffuse reflectance spectroscopy. Geoderma 132 (3–4), 273–290.

Campbell, P. M. D. M., Filho, E. I. F., Francelino, M. R., Demattê, J. A. M., Pereira, M. G., Guimarães, C. C. B., & Pinto, L. A. D. S. R., 2018. Digital Soil Mapping of Soil Properties in the "Mar de Morros" Environment Using Spectral Data. Revista Brasileira de Ciência do Solo. 42.

Carrick, S., Almond, P., Buchan, G., Smith, N., 2010. In situ characterization of hydraulic conductivities of individual soil profile layers during infiltration over long time periods. Eur. J. Soil Sci. 61 (6), 1056–1069.

Chang, C.C., Lin, C.J., 2011. LIBSVM: A library for support vector machines. ACM Trans. Intell. Syst. Technol. (TIST). 2 (3), 1–27.

Chappell, A., Webb, N.P., Guerschman, J.P., Thomas, D.T., Mata, G., Handcock, R.N., Butler, H.J., 2018. Improving ground cover monitoring for wind erosion assessment using MODIS BRDF parameters. Remote Sens. Environ. 204, 756–768.

Chepil, W.S., 1954. Factors that influence clod structure and erodibility of soil by wind: III. Calcium carbonate and decomposed organic matter. Soil Sci. 77 (6), 473–480.

Clark, R.N., Swayze, G.A., Singer, R.B., Pollack, J.B., 1990. High-resolution reflectance spectra of Mars in the 2.3-μm region: Evidence for the mineral scapolite. J. Geophys. Res.: Solid Earth 95 (B9), 14463–14480.

Conforti, M., Buttafuoco, G., Robustelli, G., Scarciglia, F., 2013. Studying the relationship between water-induced soil erosion and soil organic matter using Vis–NIR spectroscopy and geomorphological analysis: A case study in southern Italy. Catena 110, 44–58.

de Oro, L.A., Buschiazzo, D.E., 2009. Threshold wind velocity as an index of soil susceptibility to wind erosion under variable climatic conditions. Land Degrad. Dev. 20 (1), 14–21.

de Santana, F.B., de Souza, A.M., Poppi, R.J., 2018. Visible and near infrared spectroscopy coupled to random forest to quantify some soil quality parameters. Spectrochim. Acta Part A Mol. Biomol. Spectrosc. 191, 454–462.

Dotto, A.C., Dalmolin, R.S.D., Grunwald, S., ten Caten, A., Pereira Filho, W., 2017. Two preprocessing techniques to reduce model covariables in soil property predictions by Vis-NIR spectroscopy. Soil Tillage Res. 172, 59–68.

Ekhtesasi, M.R., Akhavan, G.M., Azimzadeh, H.R., Emtehani, M.H., 2003. Effects of salts on erodibility of soil by wind. Iran. J. Nat. Resourc. 56, 17–28 (In Persian).

Gholoubi, A., Emami, H., Jones, S.B., Tuller, M., 2018. A novel shortwave infrared proximal sensing approach to quantify the water stability of soil aggregates. Soil Sci. Soc. Am. J. 82 (6), 1358–1366.

Gomez, C., Lagacherie, P., Coulouma, G., 2008. Continuum removal versus PLSR method for clay and calcium carbonate content estimation from laboratory and airborne hyperspectral measurements. Geoderma 148 (2), 141–148.

Haaland, D.M., Thomas, E.V., 1988. Partial least-squares methods for spectral analyses. 1. Relation to other quantitative calibration methods and the extraction of qualitative information. Anal. Chem. 60 (11), 1193–1202.

Hong, Y., Yu, L., Chen, Y., Liu, Y., Liu, Y., Cheng, H., 2018. Prediction of soil organic matter by VIS-NIR spectroscopy using normalized soil moisture index as a proxy of soil moisture. Remote Sens. 10 (1), 28.

Janik, L.J., Forrester, S.T., Rawson, A., 2009. The prediction of soil chemical and physical properties from mid-infrared spectroscopy and combined partial least-squares regression and neural networks (PLS-NN) analysis. Chemom. Intell. Labor. Syst. 97 (2), 179–188.

Khayamim, F., Khademi, H., Stenberg, B., Wetterlind, J., 2015a. Capability of vis-NIR Spectroscopy to Predict Selected Chemical Soil Properties in Isfahan Province. J. Water Soil Sci. 19 (72), 81–92.

Khayamim, F., Wetterlind, J., Khademi, H., Robertson, A.H.J., Faz Cano, A., Stenberg, B., 2015b. Using visible and near infrared spectroscopy to estimate carbonates and gypsum in soils in arid and subhumid regions of Isfahan, Iran. J. Near Infrared Spectrosc. 23 (3), 155–165.

Kheirabadi, H., Mahmoodabadi, M., Jalali, V., Naghavi, H., 2018. Sediment flux, wind erosion and net erosion influenced by soil bed length, wind velocity and aggregate size distribution. Geoderma 323, 22–30.

Kim, I., Pullanagari, R.R., Deurer, M., Singh, R., Huh, K.Y., Clothier, B.E., 2014. The use of visible and near-infrared spectroscopy for the analysis of soil water repellency. Eur. J. Soil Sci. 65 (3), 360–368.

Knadel, M., Deng, F., Alinejadian, A., Wollesen de Jonge, L., Moldrup, P., Greve, M.H., 2014. The effects of moisture conditions—from wet to hyper dry—on visible near-infrared spectra of Danish reference soils. Soil Sci. Soc. Am. J. 78 (2), 422–433.

Kouchami-Sardoo, I., Shirani, H., Esfandiarpour-Boroujeni, I., Álvaro-Fuentes, J., Shekofteh, H., 2019. Optimal feature selection for prediction of wind erosion threshold friction velocity using a modified evolution algorithm. Geoderma 354, 113873.

Kouchami-Sardoo, I., Shirani, H., Esfandiarpour-Boroujeni, I., Besalatpour, A.A., Hajabbasi, M.A., 2020. Prediction of soil wind erodibility using a hybrid Genetic algorithm–Artificial neural network method. Catena 187, 104315.

Kovačević, M., Bajat, B., Gajić, B., 2010. Soil type classification and estimation of soil properties using support vector machines. Geoderma 154 (3–4), 340–347.

Kumar, V., Yarrakula, K., 2019. Enhancement of limestone mineral identification using Hyperion imagery: a case study from Tirunelveli District, Tamil Nadu, South India. Arabian J. Geosci. 12 (2), 38.

Kuśnierek, K., 2011. Pre-processing of soil visible and near infrared spectra taken in laboratory and field conditions to improve the within-field soil organic carbon multivariate calibration. The Second Global Workshop on Proximal Soil Sensing, Montreal, Canada. 100–103.

Lacerda, M.P.C., Demattê, J.A.M., Sato, M.V., Fongaro, C.T., Gallo, B.C., Souza, A.B., 2016. Tropical texture determination by proximal sensing using a regional spectral library and its relationship with soil classification. Rem. Sens. 8, 701.

Lagacherie, P., Baret, F., Feret, J.B., Netto, J.M., Robbez-Masson, J.M., 2008. Estimation of soil clay and calcium carbonate using laboratory, field and airborne hyperspectral measurements. Remote Sens. Environ. 112 (3), 825–835.

Li, J., Flagg, C., Okin, G.S., Painter, T.H., Dintwe, K., Belnap, J., 2015. On the prediction of threshold friction velocity of wind erosion using soil reflectance spectroscopy. Aeolian Res. 19, 129–136.

Mazidi, A., Jafari Zoj, F., Heidary, S., 2015. Simulation of dust storm events on February 28, 2009 in Fars province using WRF model. Appl. Climatol. 2 (2), 49–68 (In Persian).
Moriasi, D.N., Arnold, J.G., Van Liew, M.W., Bingner, R.L., Harmel, R.D., Veith, T.L., 2007. Model evaluation guidelines for systematic quantification of accuracy in watershed simulations. Trans. ASABE 50 (3), 885–900.
Morshedi Nodej, T., Rezazadeh, M., 2018. The spatial distribution of critical wind erosion centers according to the dust event in Hormozgan province (south of Iran). Catena 167, 340–352.
Mouazen, A.M., Kuang, B., de Baerdemaeker, J., Ramon, H., 2010. Comparison among principal component, partial least squares and back propagation neural network analyses for accuracy of measurement of selected soil properties with visible and near infrared spectroscopy. Geoderma 158 (1–2), 23–31.
Nafarzadegan, A.R., Rezaeian Zadeh, M., Kherad, M., Ahani, H., Gharehkhani, A., Karampoor, M.A., Kousari, M.R., 2012. Drought area monitoring during the past three decades in Fars province, Iran. Q. Int. 250, 27–36.
Nawar, S., Buddenbaum, H., Hill, J., Kozak, J., Mouazen, A.M., 2016. Estimating the soil clay content and organic matter by means of different calibration methods of vis-NIR diffuse reflectance spectroscopy. Soil Tillage Res. 155, 510–522.
Nelson, R.E., 1982. Carbonate and gypsum. In: Page, A.L. (Ed.), Methods of Soil Analysis, Part 2- Chemical and Microbiological Properties, 2nd edn. American Society of Agronomy, Madison, WI, pp. 81–197.
Ng, W., Minasny, B., Montazerolghaem, M., Padarian, J., Ferguson, R., Bailey, S., McBratney, A.B., 2019. Convolutional neural network for simultaneous prediction of several soil properties using visible/near-infrared, mid-infrared, and their combined spectra. Geoderma 352, 251–267.
Nourzadeh, M., Bahrami, H.A., Goossens, D., Fryrear, D.W., 2013. Determining soil erosion and threshold friction velocity at different soil moisture conditions using a portable wind tunnel. Z. Geom. 57 (1), 97–109.
Okin, G.S., 2005. Dependence of wind erosion and dust emission on surface heterogeneity: Stochastic modeling. J. Geophys. Res.: Atmos. 110, D11.
Ostovari, Y., Ghorbani-Dashtaki, S., Bahrami, H.A., Abbasi, M., Dematte, J.A.M., Arthur, E., Panagos, P., 2018. Towards prediction of soil erodibility, SOM and CaCO3 using laboratory Vis-NIR spectra: A case study in a semi-arid region of Iran. Geoderma 314, 102–112.
Ostovari, Y., Ghorbani-Dashtaki, S., Kumar, L., Shabani, F., 2019. Soil erodibility and its prediction in semi-arid regions. Arch. Agron. Soil Sci. 65 (12), 1688–1703.
Page, A.L., Miller, R.H., Jeeney, D.R., 1992. Methods of soil analysis, part 1. In: Physical and Mineralogical Methods. Soil Science Society of American Publication, Madison, pp. 1750.
Pásztor, L., Négyesi, G., Laborczi, A., Kovács, T., László, E., Bihari, Z., 2016. Integrated spatial assessment of wind erosion risk in Hungary. Nat. Hazards Earth Syst. Sci. 16 (16), 2421–2432.
Peng, Y., Knadel, M., Gislum, R., 2014. Quantification of SOC and clay content using visible near-infrared reflectance–mid-infrared reflectance spectroscopy with jack-knifing partial least squares regression. Soil Sci. 179 (7), 1–8.
Pierre, C., Bergametti, G., Marticorena, B., Abdourhamanetouré, A., Rajot, J.L., Kergoat, L., 2014. Modeling wind erosion flux and its seasonality from a cultivated sahelian surface: a case study in Niger. Catena 122, 61–71.
Post, J.L., Noble, P.N., 1993. The near-infrared combination band frequencies of dioctahedral Smectites, Micas, and Illites. Clays Clay Miner. 41, 639–644.
Raj, A., Chakraborty, S., Duda, B.M., Weindorf, D.C., Li, B., Roy, S., Sarathjith, M., Das, B., Paulette, L., 2018. Soil mapping via diffuse reflectance spectroscopy based on variable indicators: an ordered predictor selection approach. Geoderma 314, 146–159.
Ravi, S., Zobeck, T.M., Over, T.M., Okin, G.S., D'ODORICO, P., 2006. On the effect of moisture bonding forces in air-dry soils on threshold friction velocity of wind erosion. Sedimentology 53 (3), 597–609.
Rezaei, M., Riksen, M.J.P.M., Sirjani, E., Sameni, A., Geissen, V., 2019. Wind erosion as a driver for transport of light density microplastics. Sci. Total Environ. 669, 273–281.
Rezaei, M., Sameni, A., Fallah Shamsi, S.R., Bartholomeus, H., 2016. Remote sensing of land use/cover changes and its effect on wind erosion potential in southern Iran. PeerJ 4, e1948.
Rossel, R.A.V., Walvoort, D.J.J., McBratney, A.B., Janik, L.J., Skjemstad, J.O., 2006. Visible, near infrared, mid infrared or combined diffuse reflectance spectroscopy for simultaneous assessment of various soil properties. Geoderma 131 (1–2), 59–75.
Rossel, R.A.V., Behrens, T., 2010. Using data mining to model and interpret soil diffuse reflectance spectra. Geoderma 158 (1–2), 46–54.
Savitzky, A., Golay, M.J., 1964. Smoothing and differentiation of data by simplified least squares procedures. Anal. Chem. 36 (8), 1627–1639.
Schmid, T., Palacios-Orueta, A., Chabrillat, S., Bendor, E., Plaza, A., Rodriguez, M., Huesca, M., Pelayo, M., Pascual, C., Escribano, P., Cicuendez, V., 2012. Spectral characteristic of land surface composition to determination soil erosion within semiarid rainfed cultivated areas. IGARSS 2012, 7082–7084.
Shao, Y., Lu, H., 2000. A simple expression for wind erosion threshold friction velocity. J. Geophys. Res.: Atmos. 105 (D17), 22437–22443.
Shao, Y., 2008. Physics and modelling of wind erosion (Vol. 37). Springer Science & Business Media.
Sharififar, A., Sarmadian, F., Alikhani, H., Keshavarzi, A., Asghari, O., Malone, B.P., 2019. Lateral and Vertical Variations of Soil Organic and Inorganic Carbon Content in Aridisols and Entisols of a Rangeland. Eurasian Soil Sci. 52 (9), 1051–1062.
Shi, P., Castaldi, F., van Wesemael, B., Van Oost, K., 2020. Vis-NIR spectroscopic assessment of soil aggregate stability and aggregate size distribution in the Belgian Loam Belt. Geoderma 357, 113958.
Singh, J., Knapp, H.V., Arnold, J.G., Demissie, M., 2005. Hydrological modeling of the Iroquois river watershed using HSPF and SWAT 1. JAWRA J. Am. Water Resour. Assoc. 41 (2), 343–360.
Sirjani, E., Sameni, A., Moosavi, A.A., Mahmoodabadi, M., Laurent, B., 2019. Portable wind tunnel experiments to study soil erosion by wind and its link to soil properties in the Fars province, Iran. Geoderma 333, 69–80.
Stenberg, B., Rossel, R.A.V., Mouazen, A.M., Wetterlind, J., 2010. Chapter Five - Visible and near infrared spectroscopy in soil science. Adv. Agron. 107, 163–215.
Stevens, A., Nocita, M., Tóth, G., Montanarella, L., van Wesemael, B., 2013. Prediction of soil organic carbon at the European scale by visible and near infrared reflectance spectroscopy. PLoS ONE 8 (6), e66409.
Summers, D., Lewis, M., Ostendorf, B., Chittleborough, D., 2011. Visible near-infrared reflectance spectroscopy as a predictive indicator of soil properties. Ecol. Ind. 11 (1), 123–131.
Taghizadeh-Mehrjardi, R., Nabiollahi, K., Kerry, R., 2016. Digital mapping of soil organic carbon at multiple depths using different data mining techniques in Baneh region, Iran. Geoderma 266, 98–110.
Tatarko, J., 2001. Soil aggregation and wind erosion: processes and measurements. Ann. Arid Zone 40 (3), 251–263.
Terra, F.S., Demattê, J.A.M., Rossel, R.A.V., 2015. Spectral libraries for quantitative analyses of tropical Brazilian soils: Comparing vis–NIR and mid-IR reflectance data. Geoderma 255–256, 81–93.
Van der Voet, H., 1994. Comparing the predictive accuracy of models using a simple randomization test. Chemom. Intell. Laborat. Syst. 25 (2), 313–323.
Van Pelt, R.S., Hushmurodov, S.X., Baumhardt, R.L., Chappell, A., Nearing, M.A., Polyakov, V.O., Strack, J.E., 2017. The reduction of partitioned wind and water erosion by conservation agriculture. Catena 148, 160–167.
Vapnik, V. N., 1995. The nature of statistical learning. Theory.
Vicente, L.E., de Souza Filho, C.R., 2011. Identification of mineral components in tropical soils using reflectance spectroscopy and advanced spaceborne thermal emission and reflectance radiometer (ASTER) data. Remote Sens. Environ. 115 (8), 1824–1836.
Viscarra Rossel, R.A., McBratney, A.B., 1998. Laboratory evaluation of a proximal sensing techniques for simultaneous measurement of soil clay and water content. Geoderma 85, 19–39.
Visser, S.M., Sterk, G., Ribolzi, O., 2004. Techniques for simultaneous quantification of wind and water erosion in semi-arid regions. J. Arid Environ. 59 (4), 699–717.
Vohland, M., Besold, J., Hill, J., Fründ, H.C., 2011. Comparing different multivariate calibration methods for the determination of soil organic carbon pools with visible to near infrared spectroscopy. Geoderma 166 (1), 198–205.
Wan, M., Qu, M., Hu, W., Li, W., Zhang, C., Cheng, H., Huang, B., 2019. Estimation of soil pH using PXRF spectrometry and Vis-NIR spectroscopy for rapid environmental risk assessment of soil heavy metals. Process Saf. Environ. Prot. 132, 73–81.
Wang, G., Fang, Q., Teng, Y., Yu, J., 2016. Determination of the factors governing soil erodibility using hyperspectral visible and near-infrared reflectance spectroscopy. Int. J. Appl. Earth Obs. Geoinf. 53, 48–63.
Wang, J., Tiyip, T., Ding, J., Zhang, D., Liu, W., Wang, F., Tashpolat, N., 2017. Desert soil clay content estimation using reflectance spectroscopy preprocessed by fractional derivative. PLoS ONE 12 (9), e0184836.
Wiggs, G.F.S., Baird, A.J., Atherton, R.J., 2004. The dynamic effects of moisture on the entrainment and transport of sand by wind. Geomorphology 59 (1–4), 13–30.
Wilding, L.P., 1985. Spatial variability: its documentation, accommodation and implication to soil surveys, pp. 166-194. In D.R. Nielsen and J. Bouma (eds.). Soil spatial variability: Pudoc, Wageningen, Netherlands.
Xu, S., Zhao, Y., Wang, M., Shi, X., 2018. Comparison of multivariate methods for estimating selected soil properties from intact soil cores of paddy fields by Vis–NIR spectroscopy. Geoderma 310, 29–43.
Yan, Y., Li, W., Chenghuna, L., Fengming, X., Zhongjian, P., Liyu, D., 2016. Soil aggregate stability and iron and aluminium oxide contents under different fertiliser treatments in a long-term solar greenhouse experiment. Pedosphere 26 (5), 760–767.
Yan, Y., Wu, L., Xin, X., Wang, X., Yang, G., 2015. How rain-formed soil crust affects wind erosion in a semi-arid steppe in northern China. Geoderma 249, 79–86.
Zamani, S., Mahmoodabadi, M., 2013. Effect of particle-size distribution on wind erosion rate and soil erodibility. Arch. Agron. Soil Sci. 59 (12), 1743–1753.
Žížala, D., Zádorová, T., Kapička, J., 2017. Assessment of soil degradation by erosion based on analysis of soil properties using aerial hyperspectral images and ancillary data, Czech Republic. Remote Sens. 9 (1), 28.
Zobeck, T.M., Fryrear, D.W., 1986. Chemical and physical characteristics of windblown sediment I. Quantities and physical characteristics. Trans. ASAE 29 (4), 1032–1036.
Zobeck, T. M., & Van Pelt, R. S., 2014. Wind erosion. Publications from USDA-ARS /UNL Faculty. 1409.